NONLINEAR PROPAGATION OF PROFILED LIGHT BEAMS IN A SUBSONIC GAS FLOW

I.G. Zakharova, Yu.N. Karamzin, and V.A. Trofimov

M.V. Lomonosov State University, Moscow

Received July 18, 1990

Based on the use of numerical simulating, the propagation of hypergaussian and hypertubular beams in a subsonic gas flow is analyzed. It is shown that the profiled light beams experience much less nonlinear distortions. The behavior of the density perturbation profiles of a medium in the direction of the medium movement is shown to be nonmonotonic. Certain differences in the propagation of two-dimensional and slit-shaped beams are discussed.

The papers devoted to numerical studies of the beam thermal self–action in a moving nonlinear media mostly dealt with the beam propagation under conditions when $v/v_s \ll 1$, where v is the velocity of transverse movement of the medium, and v_s is the sound speed. The thermal blooming for $v/v_s \simeq 1$ has been discussed only in a few papers[1–8] and, as a rule, for Gaussian beams. For example, in Refs. 1–3 the great importance was assigned to the analysis of the density perturbations of a medium while in Ref. 4 the thermal blooming of a slit-shaped beam was analyzed. Meanwhile it is known that the profiled beams can experience much less distortions than the Gaussian beams. Therefore, it seems to be useful to study the propagation of such beams in the subsonic gas flow. In this paper we present a numerical study of thermal blooming of profiled light beams in a medium with thermal nonlinearity under conditions when the velocity of the medium movement is close to the sound speed.

PROBLEM FORMULATION AND METHOD OF NUMERICAL SOLUTION

As is well known, the process of the beam thermal self–action in a moving medium is described by a system of dimensionless equations[5]

$$\frac{\partial A}{\partial z} + i\Delta_\perp A + i\alpha\rho A = 0,$$

$$\left(\frac{\partial^2}{\partial y^2} + \left(1 - M^2\right)\frac{\partial^2}{\partial x^2}\right)\frac{\partial \rho}{\partial x} = -\Delta_\perp |A|^2, \qquad (1)$$

$$z \in (0, L_z),\ x \in (0, L_x),\ y \in (0, L_y).$$

Here functions $A(z, x, y)$ and $\rho(z, x, y)$ are the normalized complex amplitude of radiation and density variation of the ambient medium, respectively. The coordinate z coincides with the direction of beam propagation, x and y are the coordinates perpendicular to z, $\Delta_\perp = \partial^2/\partial x^2 + \partial^2/\partial y^2$, α is the coefficient equal to the ratio of the initial beam power to the characteristic power of the self–action, M is the Mach number ($0 \le M < 1$), and L_z, L_x, and L_y are the boundaries of the beam region in transverse and longitudinal coordinates, respectively.

The system of consistent equations (1) is solved under the following initial and boundary conditions:

$$A(z = 0;\ x,\ y) = A_0(x,\ y);$$

$$A(z,\ x = 0,\ y) = A(z,\ x = L_x,\ y) = A(z,\ x,\ y = 0) =$$

$$= A(z,\ x,\ y = L_y) = \rho(z,\ x = 0,\ y) =$$

$$= \frac{\partial \rho}{\partial x}(z,\ x = 0,\ y) = \frac{\partial \rho}{\partial x}(z,\ x = L_x,\ y) =$$

$$= \frac{\partial \rho}{\partial x}(z,\ x,\ y = 0) = \frac{\partial \rho}{\partial x}(z,\ x,\ y = L_y) = 0. \qquad (2)$$

As can be seen from expressions (1) and (2) the power of propagating beam remains constant.

Let us now introduce a new variable $\varphi = \partial\rho/\partial x$ and derive Eqs. (1) and boundary conditions (2) for the characteristics A, ρ, and φ. Since this procedure is quite simple, we will omit new equations. To solve this problem we shall use the pseudo–spectral symmetric finite–difference scheme, which is considered to be conservative in the sense that the total beam power obeys the power conservation law in the finite–difference approximation. Below we present a short description of this scheme, since the construction of the methods of numerical calculations makes the basis of numerical simulation widely used in atmospheric optics studies.

Let us denote the finite–difference analogs of A, ρ, and φ by A_h, ρ_h, and φ_h, respectively. Let also these values be defined at the nodes of the grid $\omega = \omega_z \times \omega_x \times \omega_y$, where

$$\omega_z = \left\{z = z_j = jh_z,\ j = 0, \ldots, N_z - 1,\ h_z = L_z/N_z\right\},$$

$$\omega_x = \left\{x = x_{k1} = k_1 h_x,\ k_1 = 1, \ldots, N_x - 1,\ h_x = L_x/N_x\right\},$$

and

$$\omega_y = \left\{y = y_{k2} = k_2 h_y,\ k_2 = 1, \ldots, N_y - 1,\ h_y = L_y/N_y\right\}.$$

0235-6880/91/01 60-7 $02.00

Let us now represent A_h and φ_h in the form of a discrete Fourier transform

$$A_h(z, x, y) = \sum_{k=1}^{N-1} A_{hk}(z)\mu_k$$

and

$$\varphi_h(z, x, y) = \sum_{k=1}^{N-1} \varphi_{hk}(z)\,\mu_k, \qquad (3)$$

where

$$k = (k_1, k_2), \quad \sum_{k=1}^{N-1} = \sum_{k_1=1}^{N_x-1} \sum_{k_2=1}^{N_y-1},$$

and

$$\mu_k = \sin(\pi k_1 x/L_x)\,\sin(\pi k_2 y/L_y).$$

The coefficients A_{hk} and φ_{hk} are derived from solving the finite–difference problem

$$\frac{\hat{A}_{hk} - A_{hk}}{h_z} - i\lambda_k \bar{A}_{hk} + i\alpha\left[\bar{\rho}_h \bar{A}_h\right]_k = 0,$$

$$\left(\lambda_{k2} + (1 - M^2)\lambda_{k1}\right)\hat{\varphi}_{hk} = -\lambda_k\left[|\hat{A}_h|^2\right]_k, \qquad (4)$$

and

$$A_{hk}(z = 0) = 4L_x^{-1}L_y^{-1}\int_0^{L_x}\int_0^{L_y} A_0(x, y)\,dxdy,$$

where

$$\lambda_k = \lambda_{k1} + \lambda_{k2}, \quad \lambda_{k1} = (\pi k_1/L_x)^2, \quad \lambda_{k2} = (\pi k_2/L_y)^2,$$

$$\hat{\varphi}_{hk}, \hat{A}_{hk} = \varphi_{hk}, A_{hk}(z_{j+1}),$$

$$A_{hk} = A_{hk}(z_j), \quad \bar{A}_{hk} = 0.5\left(\hat{A}_{hk} + A_{hk}\right),$$

$$\hat{A}_h, \hat{\rho}_h = A_h, \rho_h(z_{j+1}), \quad A_h, \rho_h = A_h, \rho_h(z_j),$$

and

$$\bar{A}_h, \bar{\rho}_h = 0.5\left(\hat{A}_h, \hat{\rho}_h + A_h, \rho_h\right).$$

The values $\left[\left|\hat{A}_h\right|^2\right]_k$ and $\left[\bar{\rho}_h \bar{A}_h\right]_k$ are derived from the formulas

$$v_k = 4L_x^{-1}L_y^{-1}\sum_{j_1=1}^{N_x-1}\sum_{j_2=1}^{N_y-1} v(z, x_{j_1}, y_{j_2}) \times$$

$$\times\,\mu_k(x_{j_1}, y_{j_2})h_x h_y. \qquad (5)$$

After finding φ_h from system (4) we can find ρ_h from a formula $\rho_h = \int_0^x \varphi_h(\xi)\,d\xi$. Since scheme (4) is nonlinear, the iteration procedure is used when we proceed to a new z layer. Let $\left[\left|\hat{A}_h^0\right|^2\right]_k = A_h$, then from the second equation of system (4) using Eq. (5) we can find $\hat{\rho}_{hk}^0$. Using the second equality of system (3), we can find $\hat{\varphi}_h^0$ and then derive $\hat{\rho}_{hk}^0$. Let us now write the first equation of system (4) in the form

$$\frac{\hat{A}_{hk}^1 - A_{hk}}{h_z} - i\lambda_k \bar{A}_{hk}^1 + i\alpha\left[\bar{\rho}_h^0 \bar{A}_h^0\right]_k = 0.$$

It should be noted that if solution (3) is valid, the conservation of the finite–difference analog of the beam power at the nodes of the grid takes place. One can readily show this multiplying $\left(\bar{A}_{hk}\right)^*$ the first equation of system (4) and then summing over all k and taking the real part of the resulting expression.

RESULTS OF NUMERICAL CALCULATIONS

Now. we proceed to the description of the computations following scheme (3)–(5). As was already mentioned above, we studied the thermal blooming of profiled laser beams, viz. hypergaussian and hypertubular beams. The amplitude distribution at the inlet into the nonlinear medium was taken to be

$$A_0(x, y) = 0.5U_0(x, y)/\|U_0(x, y)\|,$$

$$U_0(x, y) = \left[J + (1 - J)\left[(x - x_0)^m + (y - y_0)^m\right]\right] \times$$

$$\times \exp\left\{-2\left[(x - x_0)^m + (y - y_0)^m\right]\right\},$$

$$J = 0, 1, \quad m = 2, 4, 6, \quad x_0 = y_0 = 6,$$

and

$$\|U_0(x, y)\| = \int_0^{L_x}\int_0^{L_y} |U_0(x, y)|^2\,dx\,dy,$$

where $J = 1$ corresponds to Gaussian and hypergaussian initial beam profiles and $J = 0$ — to tubular and hypertubular beams.

The computer calculations were made for moderate beam power ($\alpha \le -100$) and the parameters of the propagation path $L_z = 0.2$, $L_x = L_y = 12$, and $M = 0$, 0.5, 0.7, and 0.9. The

process of simulation involved the analysis of evolution of the position of the beam's center of gravity along the x axis

$$X_{cx} = \int_0^{L_x} \int_0^{L_y} |A|^2 (x - x_0)\, dx dy,$$

the peak intensity $I_m = \max_x |A(x)|^2$ and its position x_m on the x axis, and the x–components of the beam radius

$$a_x^2 = \ln 2 \int_0^{L_x} \int_0^{L_y} |A|^2 (x - x_0)^2\, dx\, dy / \|A\|^2.$$

These parameters and the distributions of the intensity and the medium density were analyzed as a function of the parameter M, i.e., of the velocity of the medium movement.

Some of the most typical calculated results (e.g., for $\alpha = -100$) are presented in Figs. 1–3. As follows from Fig. 1*a* there occurs an increase of the beam's center of gravity shift from its position X_{cx} for $M = 0$ with the increase of the velocity of the medium movement. The shift becomes larger if the parameter M is above a certain critical value M_{cr} determined by the initial beam profile. Thus, for Gaussian and hypergaussian ($m = 6$) beams $M_{cr} = 0.6$ and 0.7, respectively, while in the case of tubular and hypertubular profiles the position of the beam's center of gravity changes insignificantly as the parameter M increases up to 0.7. It should be noted that the use of profiled beams, as in the case of slow movement of the medium allows one to decrease the shift of the beam's center from the axis of propagation. The efficiency of changing over to the profiled beams increases with increase of M. Thus, the value $|X_{cx}|$ of the Gaussian beam is more than 3 times greater than the value $|X_{cx}|$ for a hypertubular beam for $M = 0.9$. In addition it is important to note that the above dependence of X_{cx} on m becomes well–pronounced with the increase of the propagation path length (we have made calculations at z as great as 0.32).

Let us now analyze the dependences of the peak beam power and its coordinate on the velocity of the medium movement (for example, at the cross section $z = 0.2$). As follows from the numerical calculations, the peak intensity of the Gaussian beam first slightly (by a factor of 1.07) increases with the increase of M (up to 0.6) and then remains practically constant. However, the peak intensity of a hypergaussian beam at this cross section is greater than of a Gaussian beam for not only identical but also different values of the parameter M. It is important to emphasize that the peak intensity I_m of a beam with $m = 6$ monotonically increases with the increase of M, and for $M = 0.9$ it is 1.25 times above the peak intensity which is realized for slow medium movement. At the same time, the maximum value of the hypergaussian beam intensity is 1.5 times greater than I_m of a beam with the Gaussian profile at the inlet into the medium.

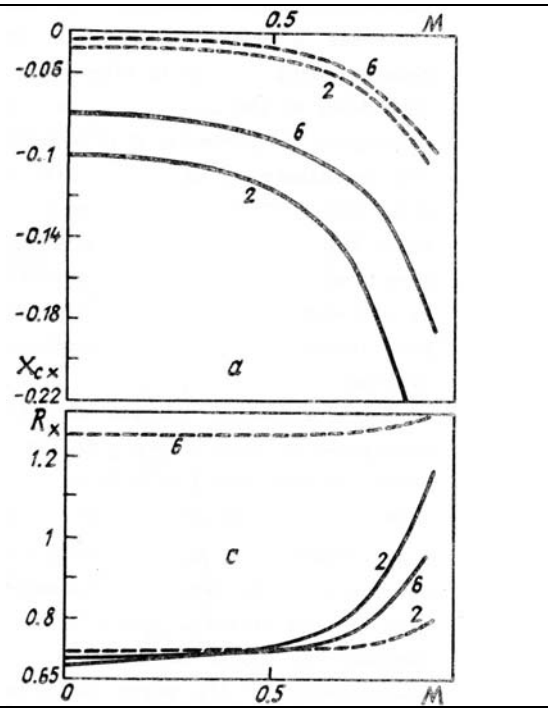

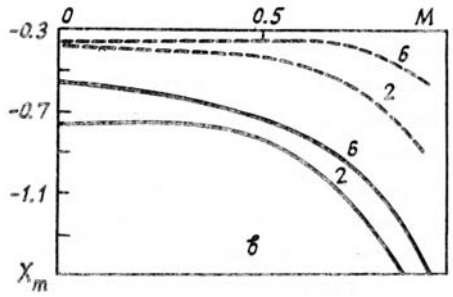

FIG. 1. Beam's center of gravity (a), coordinates of the intensity peak (b), and the x–component of the beam radius (c) as functions of the ratio of the velocity of the medium movement to the sound speed at the cross section $z = 0.2$. Solid curves represent the data for initially Gaussian beams, dashed lines for tubular ones. The values of the parameter m are shown near the curves.

The same dependences of I_m on M are realized in the case of tubular beams propagation. But in contrast to the Gaussian beams, the intensity of tubular beams monotonically increases with the increase of M. Thus, the value of I_m observed for $M = 0.9$ at a cross section $z = 0.2$ is 1.15 times greater than the corresponding value of I_m for slow medium movement. The decrease in the intensity of the hypertubular beam with $m = 6$ is equal to that for the intensity of a beam with the tubular profile at the inlet into the medium. On the whole, the intensity of tubular beams can be 1.15–2 times above the peak intensity of Gaussian beams (depending on the value of the Mach number and the beam profile). Therefore, a change over to an initially tubular beam profile is advisable also from the view point of increasing the light intensity on the detector.

It should be noted that with another cross sections along the propagation path there can occur quite different situations when the peak intensity of a hypertubular beam will be significantly greater than the value I_m of the

initially tubular intensity distribution. For example, at $z = 0.1$ for and $M = 0.9$ the value I_m with $m = 6$ is about 1.8 times greater than the value I_m with $m = 2$. This is caused by the fact that hypertubular and tubular beams are focused onto different distances. Therefore, one can focus tubular beam onto any given cross section in the nonlinear medium.

Let us now analyze the dependence of the position of the peak intensity coordinate x_m on the velocity of the medi-um movement (Fig. 1*b*). As can be seen from the figure, the position of the peak intensity shifts in the direction counter to the medium movement. In addition x_m is substantially different from the value which is realized under conditions of slow medium movement. The difference becomes noticeable already with $M = 0.6$ for the Gaussian beams, with $M = 0.5$ for hypergaussian beam, with $M = 0.7$ for tubular beams, and only with $M = 0.85$ for hypertubular beams. It cam be easily seen that the coordinate of the intensity peak of a hypertubular beam remains constant in a wide range of the velocities of the medium movement and increases only at the velocities close to the sound speed.

The analysis of the beam radii along the x axis (Fig. 1*c*) shows that the velocity of the medium movement has less of an effect on the tubular beams than on the Gaussian beams. It should be noted also that at large values of the Mach number ($M = 0.7–0.9$) the tubular beam ($m = 2$) has the smallest radius, and the parameter M has the least effect on the hypertubular beam with $m = 6$.

The analysis of the medium density perturbations and beam intensity distributions in a plane $y = y_0$ (i.e., at the beam center along the y axis, has shown that, as in Refs. 1–3, the profiles ρ along the x axis for the Gaussian beams have the zones of compression ($\rho \geq 0$) located before the center of the beam shifted in the windward direction, and the zones of rarefaction ($\rho < 0$) located behind the beam center in the direction of the medium movement. With the increase of a distance of the beam propagation in the nonlinear medium a decrease of the density perturbation amplitude occurs, and the transitional zone between the compression and rarefaction zones broadens. As the parameter M increases a monotonic increase in the medium density perturbations is observed. However, the dependence of the position of the discontinuity of density on the parameter M is nonmonotonic: first its coordinate along the x axis increases (if $M \leq 0.75$), and then it decreases. It should be noted that the nonlinear character of the Gaussian beam propagation in the nonlinear medium manifests by the asymmetry in the temporal behavior of the peak intensity and by the appearance of only one maximum.

The situation changes in the case of a hypergaussian beam with $m = 6$. As was mentioned above, in this case the shift of the beam's center from the propagation axis is smaller that, in turn, results in stronger (e.g., at the cross section $z = 0.2$) density perturbations which are less shifted from the beam's center and exhibits narrower the transitional zone. As a result, the leading edge of the pulse (with respect to the movement of the medium) is in the region of optically more thick medium that, in turn, causes the formation of aside maximum of the beam intensity, i.e., there appears a subbeam. However, the peak intensity in the subbeam is much lower than in the main maximum. The same behavior is observed with the trailing edge of the pulse that results in much greater asymmetry of the main subbeam in comparison with the case of a beam with the Gaussian intensity distribution at the inlet into the medium.

A more complicated behavior of the density perturbations and the beam intensity profile evolution takes place in the case of propagation of the tubular beams. First, the density perturbations induced by the tubular beam are approximately 1.5 times stronger than those appearing in the process of propagating the Gaussian beams. Second, for $M \geq 0.5$ nonmonotonic dependence of ρ on x is realized in the region $\rho \geq 0$ (the dashed and dot–dash lines in Fig. 2 marked by figure 2). It should be noted that $\rho(x)$ increases with a different rate with increase of M, and there appears only one maximum. The medium cross section, at which several maximums of ρ appear, is determined by the initial profile of a beam and by the Mach number.

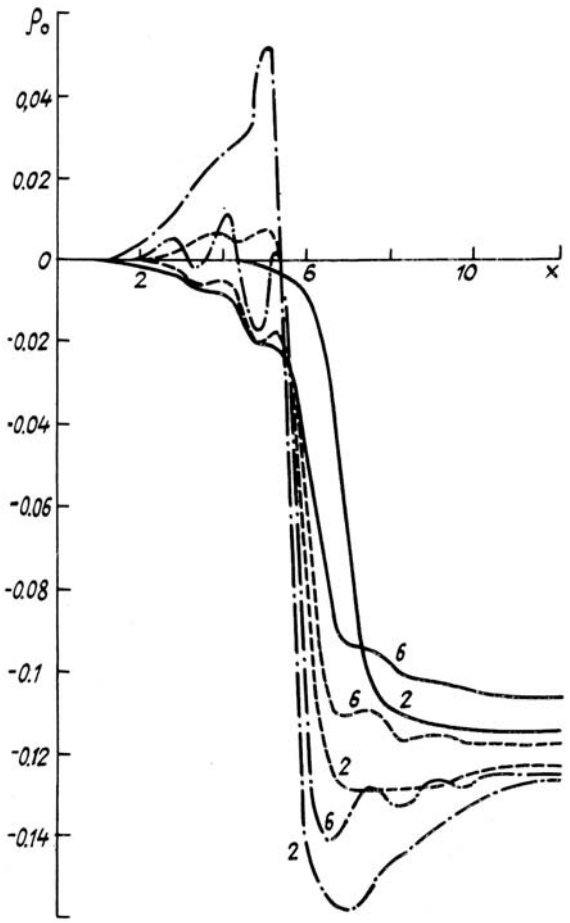

FIG. 2. The profiles of the medium density perturbations at the cross section $z = 0.2$ in a plane $y = y_0$ for the initially tubular and hypertubular beams for $M = 0$ (solid lines), $M = 0.7$ (dashed lines), and $M = 0.9$ (dot–dash lines). The values of the parameter m are shown near the curves.

It is also important to note that, in contrast to the case of hypergaussian beams, the subbeam structure is more pronounced (in the direction of the medium movement a side subbeam is formed). The asymmetry in the temporal behavior of the beam intensity distribution is manifested already at the path length $z = 0.044$, for both $m = 2$ and $m = 6$. A substantial difference for propagation of the Gaussian and tubular beams is in the fact that the central maximum of the beam intensity formed in the process of transformation of the annular beam profile first shifts (e.g., at the cross section $z = 0.044$) in the direction of the medium movement (the value of the shift being practically independent of the Mach number). In addition the asymmetry and the shift of the central intensity maximum are well pronounced for a tubular beam ($m = 2$). The

velocity of the medium movement determines the length of the path, at which the central zone of the tubular and hypertubular beams starts to shift in the direction of the medium movement, as well as the width of the central peak and of its base.

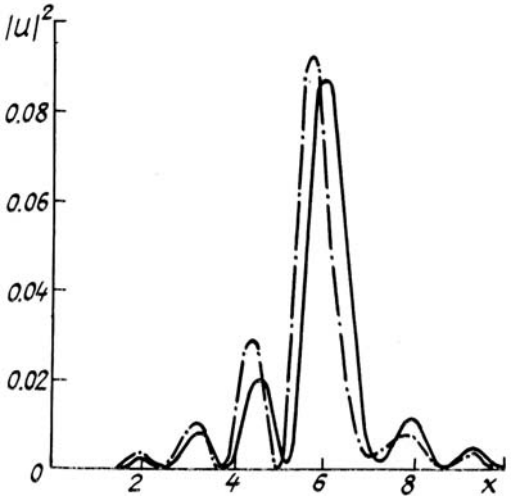

FIG. 3. Intensity distribution at the cross section $z = 0.2$ in a plane $y = y_0$ for the initially hypertubular beam ($m = 6$) for $M = 0$ (solid curve) and for $M = 0.9$ (dot–dash line).

With further propagation of a hypertubular beam (e.g., at the cross section $z = 0.1$) the formation of a subbeam structure occurs similar to that described in Ref. 9, the differences are only quantitative. Such a structure causes the modulation of density perturbations (the curves marked by figure 6 in Fig. 2) which increases with the increase of the velocity of the medium movement. As a result of the subbeam reflection from corresponding inhomogeneities of the medium, the beam profile becomes asymmetric (Fig. 3). However, in the two–dimensional case there is an asymmetry of the subbeams position relative to the central subbeam (compare with slit–shaped beams[6]): there occurs merging of the central subbeam and the next in the direction of the medium movement subbeam into a single beam. Therefore, in the two-dimensional case the nonlinear distortions are observed for lower initial power of the optical radiation.

CONCLUSIONS

1. A new method for calculating the effect of thermal blooming was proposed for light beams in a subsonic gas flow.
2. Defocusing of the profiled light beams has been investigated.
3. The analysis of the results of numerical simulations has shown that, as in the case of slow medium movement, it is advisable to change over to the profiled beams, for which, for example, the shift of the beam's center of gravity from the initial direction of propagation is much smaller than that of Gaussian beams (certain advantages also take place for another characteristics of the radiation).
4. It is shown that propagation of the profiled beams is accompanied by the formation of a side subbeam, and that the central maximum of the beam shifts in the direction of the medium movement at certain path length.
5. It is also noted that in contrast to slit–shaped beam's, the position of the subbeams of the initially two–dimensional beam are asymmetric with respect to the central one.

REFERENCES

1. D.K. Smith, Tr. IIER **65**, No. 12, 59 (1977).
2. J. Wallace and J. Pasciak, Appl. Opt. **15**, No. 5, 278 (1976).
3. J.W. Ellinwood and H. Mirels, Appl. Opt. **14**, No. 9, 2238 (1975).
4. A.N. Kucherov, Zh. Tekh. Fiz. **52**, No. 8, 1549 (1982).
5. J. Wolsh and P.B. Ulrich, in: *Laser Beam Propagation in the Atmosphere*, J.W. Strohbehn, ed. [Russian translation] (Mir, Moscow, 1981).
6. V.V. Vorob'ev et. al. , Atm. Opt. **2**, No. 2, 128 (1989).
7. K.D. Egorov, Vestn. Mosk. Univ., Fiz. Astron. **20**, No. 4, 105 (1979).
8. J.N. Hayes, Appl. Opt. **13**, No. 9, 2072 (1974).
9. I.G. Zakharova, Yu.N. Karamzin, and V.A. Trofimov, Atmos. Opt. **2**, No. 3, 237 (1989).